35th AIAA Plasmadynamics and Lasers Conference **AIAA-2004-2446**
28 Jun – 1 Jul 2004, Portland, Oregon

Comparison of Wavefront Measurement Techniques on a Two-Dimensional Heated Jet

Daniel A. Duffin [*], Stanislav Gordeyev[†], and Eric J. Jumper[‡]
Center for Flow Physics and Control
Department of Aerospace and Mechanical Engineering
Hessert Laboratory for Aerospace Research
University of Notre Dame, Notre Dame, IN, 46556-5684

A comparison of common optical wavefront measurement techniques is presented as an inter-calibration of these techniques. The sensors compared are the one-dimensional Small-Aperture Beam Technique (SABT) sensor, the one-dimensional Malley Probe, and two traditional two-dimensional Shack-Hartmann type sensors: one by Wavefront Sciences, and the other by Xinetics. The comparison was performed on a known, periodic, and repeatable optical aberration generated by a two-dimensional heated jet. The results showed good agreement between all tested wavefront sensors. The typically underappreciated effect of aperture sizing on the optical aberrations is also examined.

Nomenclature

A	=	aperture size
D	=	jet exit nozzle width
dt	=	time step
OPD	=	optical path difference
OPD_{rms}	=	root-mean-square optical path difference
OPL	=	optical path length
p'	=	pressure fluctuation
t	=	time
U_c	=	convection velocity
x, X	=	streamwise direction
x_i	=	extrapolated wavefront location
x_o	=	probe beam location
y, Y	=	spanwise direction
z, Z	=	cross-stream direction
d	=	probe beam spacing
$?t$	=	time shift for wavefront reconstruction
$?$	=	beam deflection angle
L	=	correlation length
r'	=	density fluctuation
f	=	phase error
f_{rms}	=	root-mean-square phase error

I. Introduction

WHEN an otherwise collimated laser beam is made to pass through a variable-index-of-refraction turbulent flow-field the beam's wavefront becomes aberrated, affecting its far-field point spread function. In most

[*] Graduate Research Assistant / NDSEG Fellow, 118 Hessert Laboratory, Student Member AIAA.
[†] Assistant Research Professor, 121 Hessert Laboratory, Member AIAA.
[‡] Professor, 110 Hessert Laboratory, Fellow AIAA.

applications, the beam's system utility is quantifiable by the extent to which its point spread function differs from that of a diffraction-limited pattern. When the beam's propagation distance through the turbulent medium is large compared to the beam's aperture the optical problem is referred to as an *atmospheric propagation* problem. When the propagation distance is on the order of the beam's aperture, the problem is referred to as an *aero-optic* problem.[1] Implicit in the aero-optic problem is that the aberration takes place near the beam's exit pupil, in the near-field flow around an aircraft of an airborne laser platform, for example. This implicit assumption presumes that the aberrations on the beam's wavefront will operate on the beam's intensity information over sufficient distances as to affect its far-field point spread function. There are clearly exceptions to this inference; when an imaging system is receiving an incoming optical signal, for example, the focusing optics mimic the physics of propagation to the far-field.

The role that the beam's aperture plays in the aero-optic problem is often underappreciated. The aperture places a limit (spatial filter) on the scale of the coherence lengths in the turbulent flow that are relevant to the optical problem to those scales that are on the order of a few aperture lengths and smaller.[2] This is because of another implicit assumption contained in aero-optics; some sort of tracking loop is usually assumed, often referred to as the *target loop*. In practice, this means that most aero-optical wavefront data is presented with tilt (tip-tilt) removed, frame-by-frame. In addition, piston, or average optical path length, *OPL* (or phase depending on how the wavefront is described) is also removed over the aperture, frame-by-frame. When the wavefronts are collected at sufficient bandwidth so that they are time correlated, a record of the time history of the tilt-removal can be saved and used to help quantify the bandwidth requirements of the target loop. The time history of the piston-removal is also helpful in interpreting the nature of the aberrating aero-optic flow-field.[3]

It is easy to forget that only a decade ago the aero-optic problem was a field of study relegated to statistical approaches. Turbulent flows of practical importance have coherence lengths and convective speeds that place their aberration bandwidths well above even the advanced wavefront sensors of the early 1990's. Time uncorrelated methods such as low-bandwidth wavefront sensors and interferometric techniques were able to capture instantaneous snap-shots of the aberrations, but many of these techniques were sensitive to vibration environments or relegated to interpretation due to double-pulse methodologies and the like.[1] Time correlated information was *inferred* from hot-wire data, generally recast in statistical terms, and dependent on theories developed to connect the inferred density fluctuation statistics, r', and correlation lengths, L, to root-mean-square optical path difference, OPD_{rms}. While these formulations in and of themselves have been shown to be quite accurate when properly interpreted,[1,4,5] it is now known that time-response issues in constant-current anemometry and some of the underlying assumptions about the pressure fluctuations, p', inherent in interpreting the hot-wire data incorrectly predicted the amplitude of the aero-optic aberrations.[4,5] More importantly, these techniques gave little information about spatial and temporal bandwidth requirements that would be needed to attempt to mitigate the aero-optical effects through *adaptive optics*, nor did they provide sufficient information to begin to infer the physical cause of the aberrations so that flow-control strategies might be intelligently employed in an attempt to improve the passive propagation environment.

This situation changed abruptly with the development of the SABT (Small-Aperture Beam Technique) wavefront sensor which exploited a discovery by Malley, et al. that aberrations imposed on a laser beam due to convecting structures in a turbulent flow must themselves convect through the aperture in the flow direction.[6] The basic instrument described by Malley, et al., which itself was applied to the collection of statistical information about the aberrations, was duplicated at several locations over the aperture, cross-correlated and used in new mathematical formulations to create an actual one-dimensional (in the flow direction), extremely high-bandwidth, high-spatial-fidelity wavefront sensor.[7,8] Wavefront data collected using the SABT in a serendipitous experiment carried out as a collaborative effort between Notre Dame and Arnold Engineering Development Center (AEDC) on AEDC's specially-designed compressible free shear layer facility produced the first time-resolved wavefront data at realistic flight conditions ever collected.[9] These AEDC data formed the basis for the first true understanding of the nature of the aberrating characteristics in high-speed, subsonic shear layers, and shaped the character of aero-optic research since that time.[3]

At the time of its development, no method of determining the SABT's accuracy was available, since no other high-bandwidth wavefront sensor was readily available (or perhaps even in existence) for use in an inter-calibration experiment. The SABT's accuracy was constructed from numerical simulations of an aberrating flow. In an attempt to experimentally determine its accuracy for a given flow, a heated-jet was acoustically forced over a 14 hour period and constant-current anemometry methods were used to construct a phase-averaged, pseudo-time-resolved temperature field through the jet. These temperature data were then used to construct a similar index-of-refraction time series, from which a time series of wavefronts were computed for the purpose of comparing them to an SABT time series collected in a fraction of a second. Instead of providing a fiducial set of wavefronts for comparison to the

SABT wavefronts, the comparison revealed shortcomings in the presumed bandwidth of the constant-current anemometer which were later painfully accounted for through additional processing of the raw anemometry data.[4,5]

Since that time, a number of new wavefront instruments have been developed and are in use by the Aero-Optics Group at Notre Dame that include a Wavefront Sciences' CLAS-2D 30 Hz Shack-Hartmann wavefront sensor, a relatively-high-bandwidth (~1 kHz) Xinetics Shack-Hartmann wavefront sensor, the SABT wavefront sensor, and a relatively new maturation by Notre Dame of Malley's original instrument referred to as a Malley Probe.[10] The purpose of this paper is to describe results from a comparison of these sensors again using the acoustically-forced heated jet facility. In so doing, we will attempt to point out the advantages and limitations of each of the instruments, as well as how one goes about properly comparing the instruments with a special emphasis placed on the importance of selecting the aperture.

II. Two-Dimensional Heated Jet Facility

The heated-jet facility is shown schematically in Fig. 1. It consists of a plenum chamber pressurized above atmospheric pressure by a squirrel-cage type blower. After passing through filters and a slight contraction, air enters a rectangular duct with a series of heaters located approximately 1 m from its entrance and 1 m from a ninety degree finned bend so that the heated air is now moving vertically in a rectangular duct with filters and flow straighteners as shown in Fig. 1. The flow then passes through a 16-to-1 two-dimensional nozzle to an exit nozzle width, *D*, of ½ in. (1.27 cm). The heated jet leaves the nozzle with a core velocity of 7 m/s. The detailed fluid mechanic measurements for this jet can be found in Ref. 11.

Figure 2 shows a schematic of the exit plane of the nozzle. The left side of the figure shows a view normal to the span of the jet (the aero-optic view) showing the span dimension, 30 cm, and the end plates aligned in the flow direction to help reduce three-dimensional effects that would otherwise be present if the jet were to be uncontained. The right side of the figure shows a view along the cross-stream direction of the jet showing a number of important details. First, the jet exit plane forms a solid floor that extends for 0.52 m in each direction from the nozzle gap. Second, the location and orientation of a speaker used to force the flow is shown; this speaker is located in the exit plane 1 m from the center line of the nozzle.

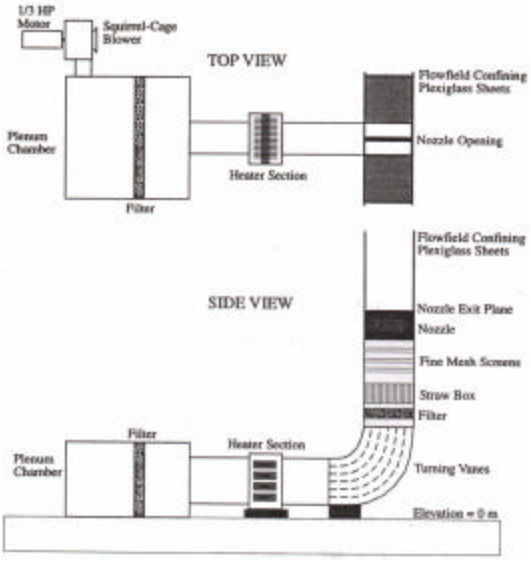

Figure 1. Two-dimensional heated jet facility.[11]

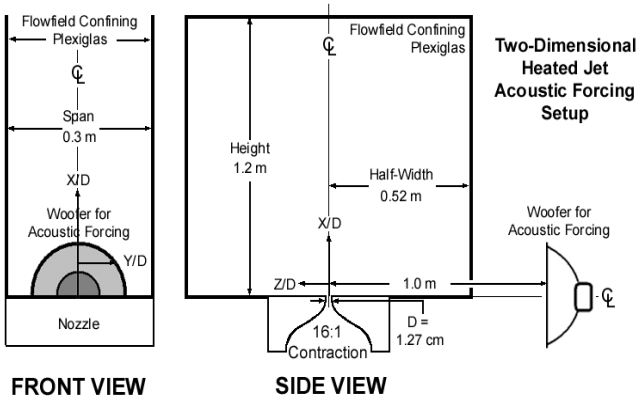

Figure 2. Heated jet exit plane schematic.

A. Jet's Response to Acoustic Forcing

The details of the jet's response to acoustic forcing will be given in a forthcoming paper.[12] It is sufficient here to briefly describe the jet's characteristics used for the comparisons reported here. The acoustic forcing was provided by a Pyramid PWFX107 600W 10" woofer located as shown in Fig. 2. The speaker was driven by a Crown CE2000 PA amplifier with an input provided by an Agilent Model 33120A function/arbitrary waveform generator. In the present case the jet was forced with a 240 Hz sine waveform.

The jet's response to the 240 Hz forcing was to regularize the jet's most-unstable Kelvin-Helmholtz instability in the jet's two bound shear layers. Depending on the amplitude of the acoustic signal, the first roll-up can be adjusted closer or further away from the nozzle exit plane. The forcing also regularizes the first pairing resulting in the formation of 120 Hz sub-harmonic, larger-coherence-length flow structures; however, this regularization is slightly less robust than the first roll-up. In order to provide the best 120 Hz regularization the amplitude of the acoustic signal caused the 240 Hz roll-up to occur somewhat closer to the exit plane than used and reported in earlier studies, which concentrated primarily on the 240 Hz structures.[4,8] In these earlier studies, the two-dimensional heated jet facility was acoustically forced in a manner similar to this present experiment. A smoke visualization of the jet and the phase-locked-averaged temperature field collected for the forced jet is shown in Fig. 3. Figures 4 and 5 show the effect that the acoustic forcing had on the jet's *OPD* pattern. Figure 4 is the heated jet's *OPD* pattern without acoustic forcing. One should note that the *OPD* peaks are quite random and while there is a certain temporal frequency to this pattern, there is also a large standard deviation about this frequency. Figure 5 shows that acoustic forcing regularizes both the amplitude of the *OPD* as well as the temporal frequency of the pattern. It is this predictable, repeatable *OPD* pattern that was used to inter-calibrate the wavefront measurement devices for this study.

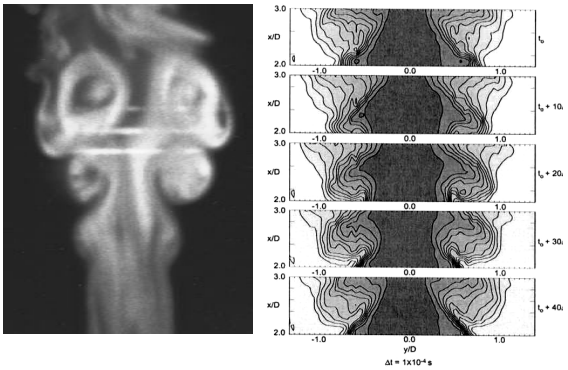

Figure 3. Smoke visualization of the two-dimensional heated jet (left), and phase-averaged temperature profiles of the jet (right).[4]

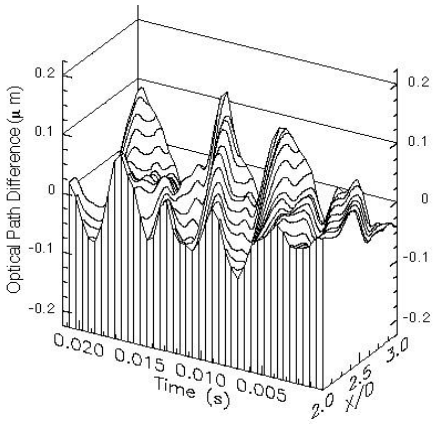

Figure 4. Time series of experimentally-measured *OPD*'s from propagation through a two-dimensional heated jet without acoustic forcing.[8]

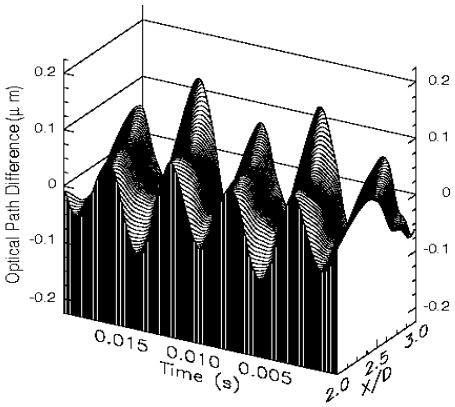

Figure 5. Time series of experimentally-measured *OPD*'s from propagation through a two-dimensional heated jet with acoustic forcing.[13]

III. Wavefront Sensors

A. Malley Probe

The Malley Probe is an optical instrument that can make direct, accurate measurements of dynamically-distorting wavefronts, including the character of the *OPD(t)* over some aperture size (determined during the testing). By moving the instrument, an entire large aperture can be optically characterized. This characterization includes not only a measurement of OPD_{rms}, but also the spatial frequencies (coherence lengths) and temporal frequencies of the aberrations. The instrument itself is a further development by Notre Dame of an instrument described in a paper by Malley, et. al.[6] In that paper, a working instrument was developed and applied to an aero-optical flow and shown to be consistent with OPD_{rms} estimates made using a limited number of interferograms for the same flow-field. The Notre Dame, Malley-derivative, sensor is an advancement over the one described in Ref. 6.

The Notre Dame instrument consists of two closely spaced small-aperture beams (beam diameter ~ 1 mm spaced 23 mm apart and aligned in the streamwise direction); the second beam is used to extract phase or

convection velocity, U_c, data contained on the beam-deflection angles by cross-correlating the two signals and obtaining the time delay for maximum correlation. Knowing the distance between the two beams and this delay time, the convection velocity of the optical aberrations can be computed. A more-robust method of determining the convection velocity using a spectral method is described in Ref. 10. As described in Refs. 7-8, the deflection angle of the probe beam is the spatial derivative of the wavefront for a larger-aperture beam if that large-aperture beam were aberrated by the same flow at the location of the probe beam. The convection velocity is then needed to unfold the *OPL* using the fact that the aberrations "convect" with the fluid structures,

$$OPL(x,t) = \int_{t_o}^{t} \left(\frac{dOPL}{dx} \right)_{x_o} \left(\frac{dx}{dt} \right) dt = \int_{t_o}^{t} [-?(t)] U_c \, dt. \tag{1}$$

Once $OPL(x_o, t)$ is known (typically at bandwidths of up to 150 kHz) at the single probe location, x_o, a Taylor's frozen flow hypothesis can be made to project *OPL* upstream and downstream by trading time and position as,

$$OPL(x_i, t) = OPL(x_o \mp U_c \Delta t_i, t), \tag{2}$$

where

$$\Delta t_i = \frac{|x_i - x_o|}{U_c}, \tag{3}$$

where in Eq. (2) the "-" is for upstream construction and the "+" is for downstream construction (i.e., upstream wavefront information has not arrived at the probe location by time t). Once the extrapolated *OPL* is known for all locations, up and downstream from the measurement location an aperture size, A, may be constructed centered on the probe location and extending up and downstream from that location a distance $A/2$. Clearly, the larger A is chosen, the less accurate the wavefront reconstruction; however, Hugo and Jumper have shown that even though the actual wavefronts are inaccurate, all of the relevant optical information can be extracted from the extrapolated wavefront over a surprisingly-large aperture.[7] Once $OPL(x, t)$ has been extrapolated over the aperture the mean *OPL* over the aperture at each instant in time can be removed, frame-by-frame, to give $OPD(x, t)$. This time history of the mean *OPL*, or pedestal, can be saved for later interpretation of the data. From the instant to instant *OPD*'s, the OPD_{rms} can be computed directly or with tilt removed. Again, a time history of the tilt-removal can be saved for later interpretation of the data.

Malley Probe data are also meaningful in a heavy vibration environment because the raw data are in the form of a time series of wavefront slope data (jitter data). The spectral method for extracting the convection velocity referred to earlier also provides information about the band of frequencies (usually less than 500 Hz) where the jitter on the two beams is not convecting; such non-convecting jitter signals infer that they are caused by vibration. Knowing the bandwidth where the vibrations reside means that these can be filtered out of the data using a high-pass filter. Usually the aero-optic data is higher than the vibration filter cut-off frequency, so that no meaningful aero-optical information is lost.

Given a wavelength of interest, the time series of *OPD* over the aperture can be turned into instantaneous phase, $f(x, t)$ over the aperture in the flow direction. Depending on other information available to infer the spanwise character of the wavefront (i.e., the flow is assumed to be two-dimensional, for example), frame-by-frame realizations of the far-field intensity pattern and Strehl ratio can be computed using *Fourier Optics*. The time-averaged Strehl ratio can then be formed and compared to the time-averaged Strehl ratio obtained using the usual *large-aperture approximation*, which has been noted to be accurate only if the optical aberrations are one-tenth of a wave or less.

A simplified schematic of the optical arrangement of a Malley Probe is shown in Fig. 6.

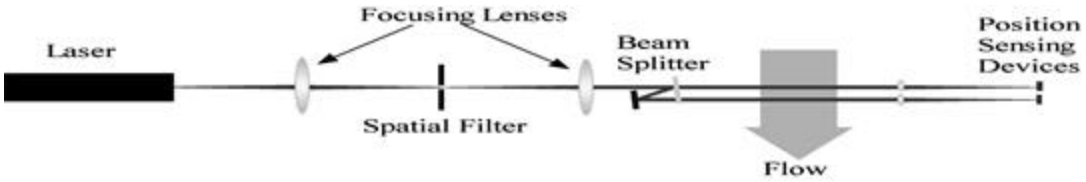

Figure 6. Schematic of a Malley Probe layout.

A typical Malley Probe set-up is shown in Fig. 7, which shows a He-Ne laser, a pin-hole and focusing optics, a beam splitter that splits the beam into two closely-spaced beams, beam-steering optics to take the beams to and return them from the region of interest, focusing lenses and finally position sensing devices placed at the focal plane of the two focusing lenses.[14] The position sensing devices are shown in Fig. 8.

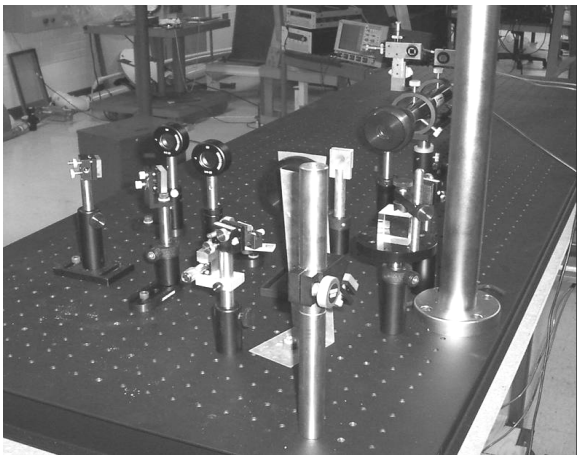

Figure 7. Optical bench layout of a Malley Probe.

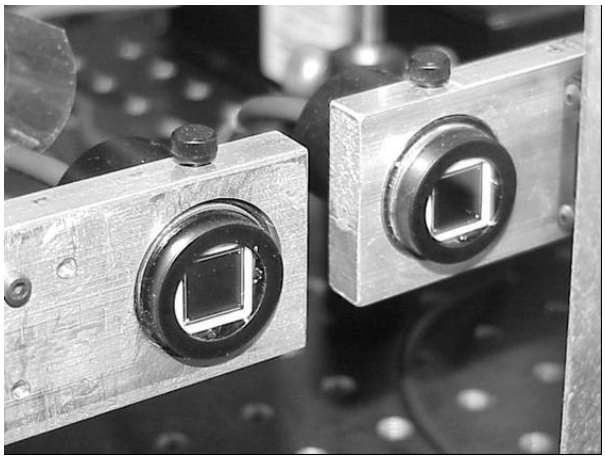

Figure 8. Position sensing devices.

B. SABT Wavefront Sensor

The SABT wavefront sensor is similar to the Malley Probe in terms of the physics it exploits in order to construct a wavefront. Like the Malley Probe it is capable of measuring wavefronts only in the streamwise direction, although scanning beams have been used to develop a full two-dimensional sensor.[15] Whereas the Malley Probe extrapolates a pseudo-wavefront up and downstream from its probe location, the SABT wavefront sensor is able to construct an accurate wavefront over the entire aperture.[7] The SABT sensor does this by placing beams further apart than the Malley Probe. Whereas in the Malley Probe case the beams are so close that the Taylor's frozen flow hypothesis is essentially true, in the SABT case the fact that when the beams are placed at further distances apart the flow, and thus the aberrations, are known to evolve is exploited. As described in Ref. 8, although the beams are separated by sufficient distance to capture this evolution, the actual distance of separation is determined by the flow

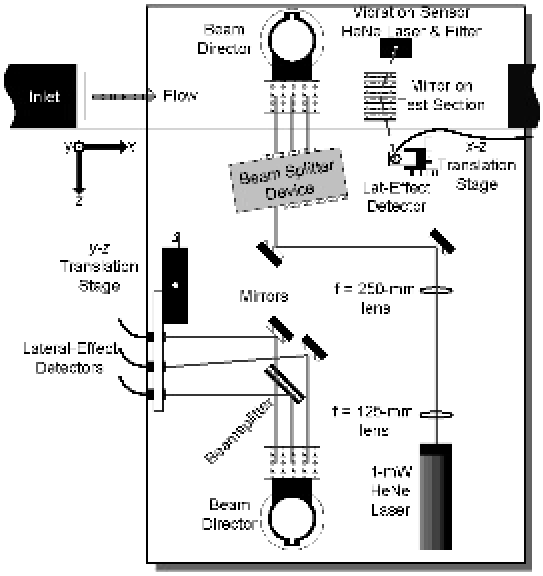

Figure 9. SABT Wavefront Sensor layout.

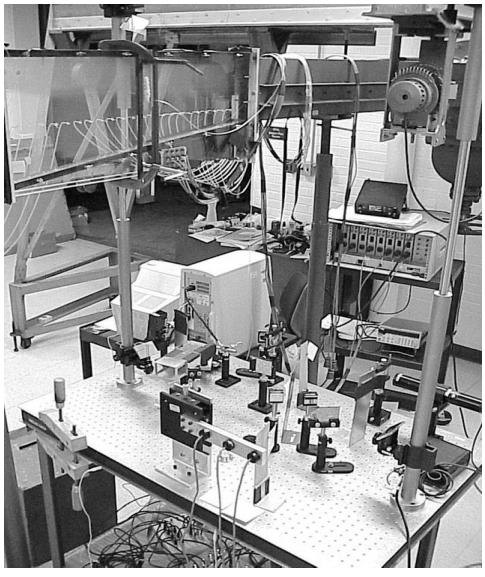

Figure 10. Transonic shear layer facility with SABT equipment on optical bench.

as a trade off of wavefront accuracy versus the number of beams used over the aperture. Once the number of beams is chosen, the SABT represents a sparse sensor array which makes it possible to capture wavefronts at bandwidths up to the electronics limit, typically up to 150 kHz for the electronics we use. A typical optical bench layout for an SABT wavefront sensor is shown in Fig. 9. The layout in Fig. 9 was used with the tunnel shown in Fig. 10, and looks similar to the Malley probe setup shown schematically in Fig. 6 but with larger beam spacing and an additional beam; note that only three beams were needed, in this case, for a 10 cm aperture.[16]

The equations for reconstructing the wavefront between SABT probe beams are more complicated than for a Malley Probe reconstruction and involve non-stationary cross-correlations and weighted averaging; however, the basic principles are represented by Eq. (1) – Eq. (3). The SABT wavefront sensor has been used for many aero-optic applications and the reader is directed to Refs. 7-8 for further details.

C. Wavefront Sciences Wavefront Sensor

The Wavefront Sciences wavefront sensor is a traditional Shack-Hartmann sensor.[17] The sensor head itself is a CCD camera (without a lens) with, in the present case, a 33 x 44 lenslet array permanently aligned and mounted over the CCD array at the lenslet focal distance. The camera is framed by an off-the-shelf frame grabber, which in the present case can be single-frame externally triggered, or can be run at a framing rate of 30 Hz. Clearly, the framing rate is insufficient to time resolve aero-optical flows of any practical importance; however, in the present case, with the heated jet acoustically forced as described in an earlier section, a pseudo-time-resolved time series of phase-locked-averaged wavefronts can be collected for the purpose of comparison with other time-resolved wavefront-measuring instruments. Otherwise, when used in conjunction with an SABT or Malley Probe sensor, many time-uncorrelated wavefronts can be collected along with the time-resolved data to serve as a database for inferring the spanwise correlations used to construct far-field patterns, as discussed earlier.

It is important to note that both pedestal and tilt must also be removed from the two-dimensional wavefronts. Further, when used as a "sanity check" for interpretation of the Malley-Probe data, a streamwise cut through the wavefront must first be made and its mean and tilt removed. It is important to note that non-time-resolved wavefronts contain no frequency information, and vibration contamination can only be removed by assuming that the average tilt over the aperture is due solely to vibration.

D. Xinetics Wavefront Sensor

In addition to the Wavefront Sciences wavefront sensor, Notre Dame also owns a higher-bandwidth, but lower-spatial-resolution Shack-Hartmann wavefront sensor as part of an *adaptive optics* system designed and assembled by Xinetics, Inc. This wavefront sensor consists of a Dalsa CCD camera (without a lens) that can be framed at 978 Hz, with a 11 x 11 lenslet array aligned and mounted at its focal length above the CCD array. In the present case, with the heated jet forced at 240 Hz, this allows for approximately four frames per passage frequency of the fundamental and eight for the sub-harmonic.

IV. Wavefront Results

A. SABT Sensor and Malley Probe Wavefront Realizations

1. *Selection of SABT Sensor Probe Beam Spacing (d/D)*

As described above, the main tradeoff with the SABT sensor is accuracy versus number of sensors over the aperture. Following the procedure outlined in Ref. 8, a cross-correlation of two probe beams was performed for a range of probe-beam spacings, *d/D*. Cross-correlations for the forced jet with the probe beams centered on *X/D* = 1.5 are shown in Fig. 11. It should be noted that as the probe beam spacing increases the maximum normalized cross-correlation coefficient decreases. Using the relationship between cross-correlation value and wavefront accuracy given in Ref. 8, the expected error of the *OPD* measurement can be determined. From Fig. 11, the maximum cross-correlation coefficient for a spacing of *d/D* = 0.5 is 0.43, from Ref. 8 this corresponds to a conservative estimate of no more than an error of 7.8% of peak-to-peak amplitude in the *OPD* can be expected. Similarly, for a probe beam spacing of *d/D* = 1.0 the maximum value of the normalized cross-

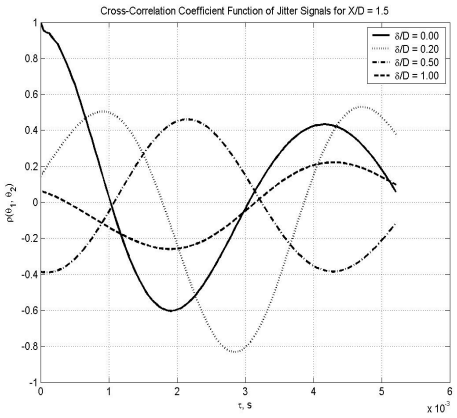

Figure 11. Cross-correlation of probe beams as a function of beam spacing.

correlation coefficient is 0.23, corresponding to a maximum error of roughly 12%. Since an error of 12% is acceptable in present study, a probe beam spacing of d/D = 1.0 was selected.

2. SABT Sensor and Malley Probe Set-Up

The probe beams for the SABT sensor were placed one diameter apart as discussed above. The upstream beam was placed at X/D = 1.0 and the downstream beam was placed at X/D = 2.0. For a strict SABT wavefront construction this corresponds to an aperture of 1.0 X/D. This aperture size captures approximately one cycle of the 240 Hz aberrating structures present in the region for the forced heated jet. For the Malley Probe, the probe beam was placed at X/D = 1.5, placing it at the center of the SABT aperture; the second Malley Probe beam was placed d/D = 0.25 downstream from the first probe beam. Time series of data were taken and analyzed with the algorithms described above. Both sets of data were extrapolated to an overall aperture of X/D = 0.5 to 2.5. This overall aperture could then be re-apertured to any desired aperture centered on X/D = 1.5.

3. Comparison of SABT and Malley Probe Results

For comparison purposes the aperture selected for the direct comparison of these two techniques was X/D = 1.0 to X/D = 2.0. Figure 12 shows representative instantaneous measurements of OPD over 360 degrees of phase for the aberration cycle with the 240 Hz acoustic forcing. Due to the acoustically-forced regularization of the heated jet's optical aberrations, the OPD repeats itself every 240 Hz (or 360 degrees of phase). Figure 12 shows excellent agreement between the SABT sensor and Malley Probe results.

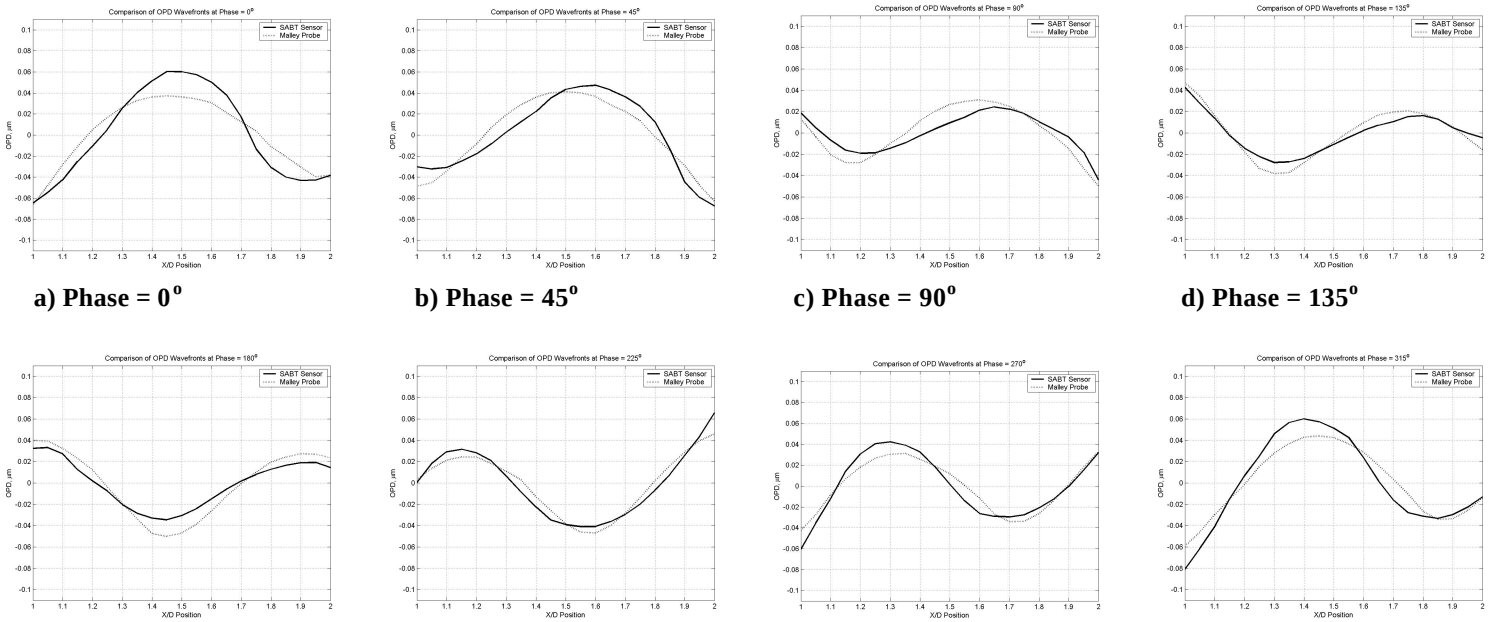

a) Phase = 0° **b) Phase = 45°** **c) Phase = 90°** **d) Phase = 135°**

e) Phase = 180° **f) Phase = 225°** **g) Phase = 270°** **h) Phase = 315°**

Figure 12. Comparison of SABT sensor wavefronts (solid line) to Malley Probe wavefronts (dotted line) from streamwise position of X/D = 1.0 to X/D = 2.0 for a variety of phase angles (OPD scale in µm).

4. Effect of Phase-Averaging the SABT Sensor Data

As a measure of how well the flow was forced, many cycles of SABT OPD realizations were phase-lock-averaged. Figure 13 shows the comparison between the single-cycle realizations and the phase-averaged realizations. Although the general comparison is good, there are clear indications that there are slight variations from one cycle to the next that in some cases exceed the differences between the SABT realizations and those of the Malley Probe shown in Fig. 12.

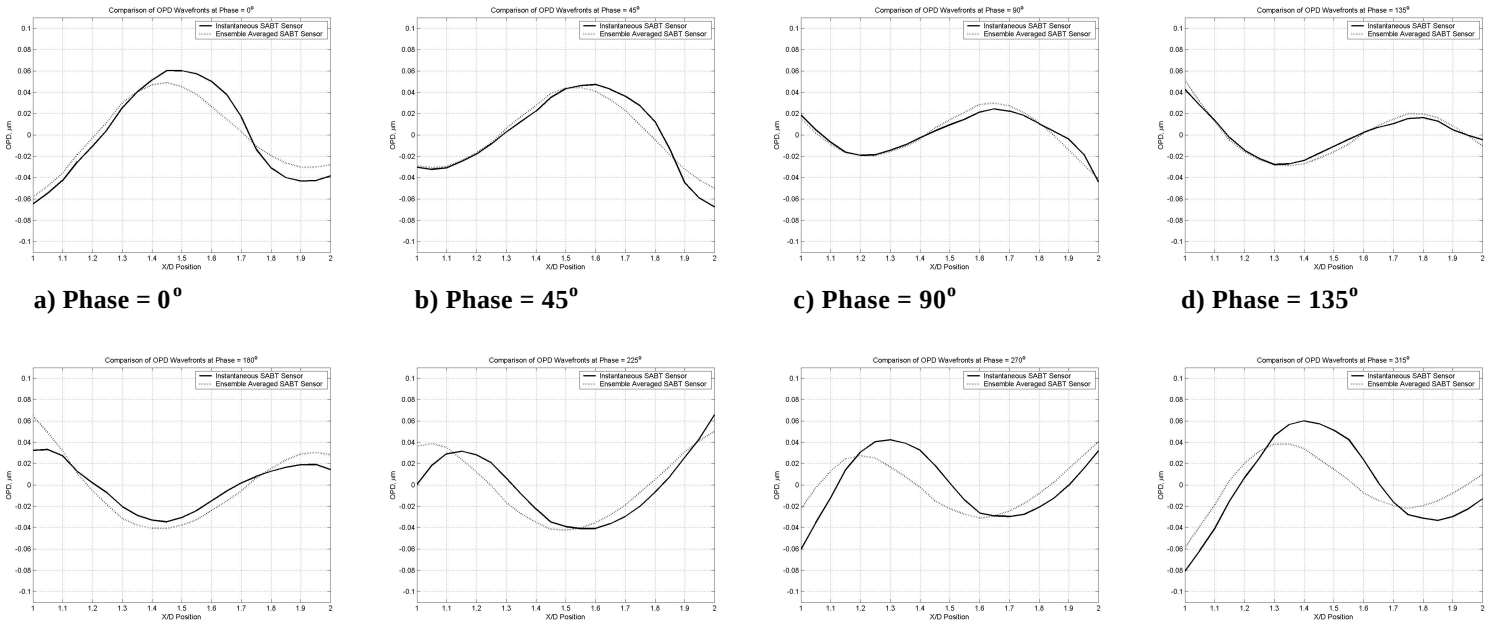

a) Phase = 0° **b) Phase = 45°** **c) Phase = 90°** **d) Phase = 135°**

e) Phase = 180° **f) Phase = 225°** **g) Phase = 270°** **h) Phase = 315°**

Figure 13. Comparison of instantaneous SABT sensor wavefronts (solid line) to phase-locked-averaged SABT sensor wavefronts (dotted line) from streamwise position of *X/D* = 1.0 to *X/D* = 2.0 for a variety of phase angles (*OPD* scale in µm).

B. Instantaneous Two-Dimensional Wavefront Realizations

1. Wavefront Sciences Wavefront Sensor

The results in Fig. 14 show typical instantaneous realizations of two-dimensional wavefronts collected with the Wavefront Sciences system. When the jet is acoustically locked, as in these experiments, the presumption is that the jet becomes two-dimensional, that is to say the flow structure in the x-direction is repeated at all span, y, locations. The two-dimensional wavefronts in Fig. 14 indicate that this presumption, although not perfect, is closely approximated by the flow. Further, the convective nature of the aberration through the aperture is clearly apparent in the realizations.

In order to compare these Wavefront-Sciences results to the one-dimensional results obtained with the SABT sensor and the Malley Probe, a one-dimensional slice in the central location of the two-dimensional wavefronts must be made. These now one-dimensional wavefronts must then have their mean and tilt removed over an appropriate aperture. The one-dimensional comparisons of these two-dimensional wavefronts to the SABT sensor and the Malley Probe are presented in a subsequent section.

2. Xinetics Wavefront Sensor

Since the Xinetics wavefront sensor operates at 978 Hz, only four realizations of an aberration cycle are captured over that 240 Hz cycle, each realization separated by approximately 90 degrees. Unlike the Wavefront Sciences sensor, the Xinetics sensor is free-running so that attempting to capture phase-locked-averaged realizations is impractical. Instead, individual frames were examined until a frame closely matching one of the phase angle realizations in Fig. 14 was found (the frame found matched the 45 degree case of Fig. 14). The next successive three frames were then presumed to represent approximately the next three 90°-separated frames at 135, 225 and 315 degrees, it was these frames that were compared to the Wavefront Sciences realizations at the same phase angles. This set of four realizations from the Xinetics wavefront sensor is given in Fig. 15. Like the SABT and Malley Probe wavefronts, the Xinetics wavefronts represent realizations of a single disturbance convecting through the aperture.

The non-circular shape of the wavefronts, most notable in the bottom "contour" views, is a consequence of a miss-register of the circular beam to the 11 x 11 sub-aperture array of the sensor, and carries no significance for the

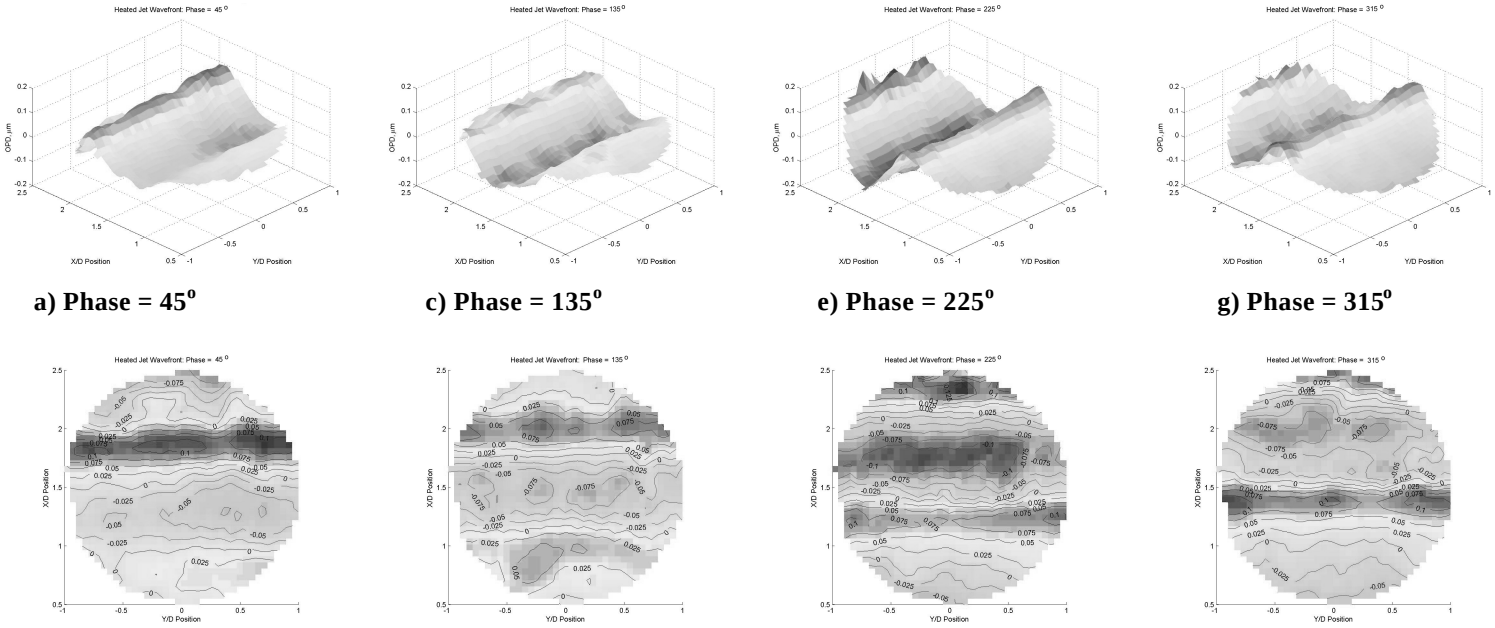

a) Phase = 45° **c) Phase = 135°** **e) Phase = 225°** **g) Phase = 315°**

b) Phase = 45° **d) Phase = 135°** **f) Phase = 225°** **h) Phase = 315°**

Figure 14. Typical instantaneous wavefronts obtained with the Wavefront Sciences CLAS-2D wavefront sensor at various phase angles: surface plots (top) and contour plots (bottom); (-1.0 < *Y/D* < 1.0; 0.5 < *X/D* <2.5; *OPD* scale in mm).

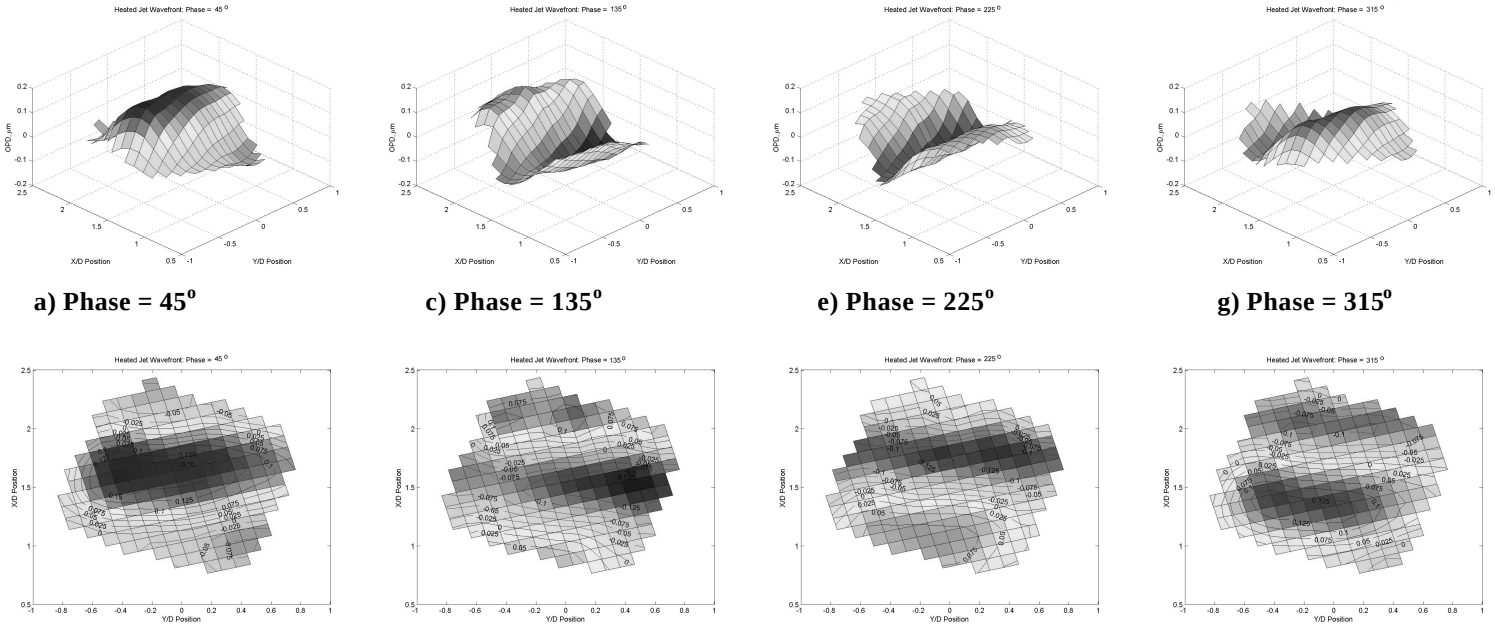

a) Phase = 45° **c) Phase = 135°** **e) Phase = 225°** **g) Phase = 315°**

b) Phase = 45° **d) Phase = 135°** **f) Phase = 225°** **h) Phase = 315°**

Figure 15. Typical instantaneous wavefronts obtained with the Xinetics wavefront sensor at various phase angles: surface plots (top) and contour plots (bottom); (-1.0 < *Y/D* < 1.0; 0.5 < *X/D* <2.5; *OPD* scale in mm).

purpose of comparison to any other wavefronts. As to the character of the wavefronts, once again both the nearly-one-dimensional character of the wavefronts for this single convecting aberration and its convective character are apparent in the Xinetics wavefronts as they were for the Wavefront Sciences wavefronts. One-dimensional wavefronts for the purpose of comparison in a later section to the SABT and Malley Probe wavefronts must be constructed in the same way as described for the Wavefront Sciences two-dimensional wavefronts.

3. Comparison of the Wavefront Sciences and Xinetics Two-Dimensional Wavefronts

Before making overall comparisons of all four wavefront sensors, it is useful to compare the two-dimensional wavefronts from the Wavefront Sciences and Xinetics sensors. First, as noted in Section IV-B.2, the non-circular shape of the Xinetics wavefronts has no significance. There some clear similarities in the two sets of wavefront realizations. Close inspection of the two sets show that the peak-to-peak amplitude of the wavefronts is clearly of the same order (this will be compared more closely in the next section). The major features are also in their proper location for each of the four phase angles, although this is to be expected based on the best-fit exercise described in the last section. There are also some clear differences in the two sets. The most noticeable difference is the sharp character of the Wavefront Sciences wavefronts compared to the Xinetics wavefronts. This softening of the wavefronts by the Xinetics sensor is a direct consequence of the sub-aperture resolution; the eleven sub-apertures of the Xinetics system place a spatial filter on the higher-order aberrations, which the thirty-three sub-apertures of the Wavefront Sciences sensor are able to resolve.

C. Comparison of Wavefront Measurement Techniques

A comparison of all four wavefront-sensing techniques over an aperture from X/D = 1.0 to X/D = 2.0, the strict SABT aperture length, is given in Fig. 16. Note that the Xinetics wavefronts are only at 45, 135, 225 and 315 degrees for the reasons explained in Section IV-B.2, and that the Wavefront Sciences wavefronts have been phase-locked-averaged over 500 cycles. Figure 16 not only shows that the Wavefront Sciences and Xinetics peak-to-peak amplitude measurements are of the same order; the averaging of the Wavefront Sciences wavefronts do not show any clear trend to either exceed or under represent the peak-to-peak amplitudes of the wavefront realizations when compared to the Xinetics sensor. In fact, over this aperture size a detailed phase-angle–by–phase-angle comparison reveals no clear representative trends that would distinguish any one of the methods from the others. This equivalence of methods also extends to statistical measures of the wavefronts. Structure size, or coherence length, is preserved in all the techniques and OPD_{rms} are similar, 0.028 μm for the SABT sensor, 0.028 μm for Malley Probe, 0.025 μm for the Wavefront Sciences sensor, and 0.025 μm for the Xinetics wavefront sensor, all within 12% of one another. It is interesting to note that the OPD_{rms} reveals a slight decrease in amplitude of the Wavefront Sciences and Xinetics wavefronts due in all probability to the averaging of the one and the low spatial resolution of the other, respectively. Over this aperture size and for this particular aberrating flow-field there is no clear best sensor.

1. Effect of Aperture on Wavefront Comparisons

Just as the Malley Probe extends the wavefront information upstream and downstream by presuming that the frozen-flow hypothesis is strictly true, the aperture of the SABT sensor can be extended upstream and downstream from its strict limits by projecting slope information upstream and downstream from their probe beam locations. This has been done in Fig. 17. Also shown in Fig. 17 are the full aperture one-dimensional slices through the Wavefront Sciences and Xinetics wavefronts. It is clear in the Fig. 17 comparison that there begins to be discrepancies between methods, primarily due to the breakdown in the frozen-flow hypothesis. The extrapolated SABT and Malley wavefronts do a descent job predicting the wavefront in the downstream direction but grossly over predict the wavefronts upstream of the probe beams. This can be attributed to the fact that the flow structures are evolving rapidly in those regions; initial vortex roll-up is occurring in the upstream region while vortex pairing is occurring in the downstream region.[12]

The OPD_{rms} over these frames for each respective wavefront sensor are: SABT sensor, 0.038 μm; Malley Probe, 0.035 μm; Wavefront Sciences sensor, 0.037 μm; Xinetics wavefront sensor, 0.030 μm. For this aperture size the OPD_{rms} is still within about 26%, with the large discrepancy being with the Xinetics sensor. This error is most likely due to the effect of removing the mean over the aperture. When the slope is clearly missed at the edge of the aperture and projected beyond the actual wavefront, that error shows up in the mean OPL over the aperture. Also, the larger aperture allows for larger correlation lengths to effect the wavefront measurement, thus inflating the value of OPD_{rms}.

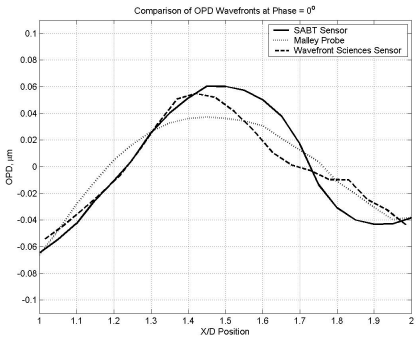

a) Phase = 0°

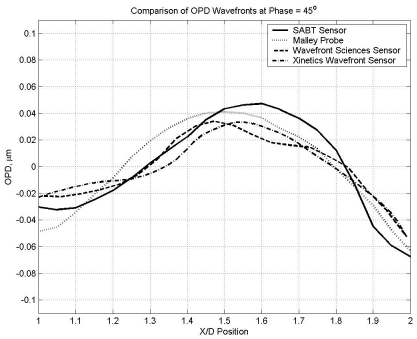

b) Phase = 45°

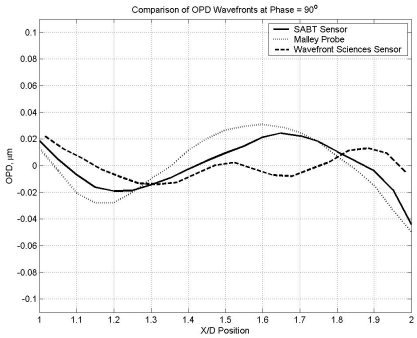

c) Phase = 90°

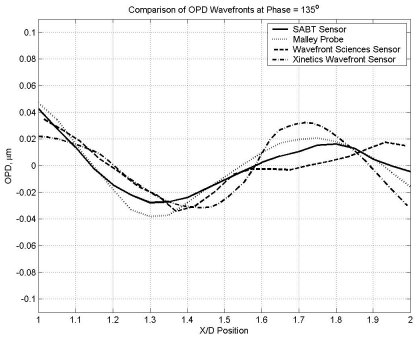

d) Phase = 135°

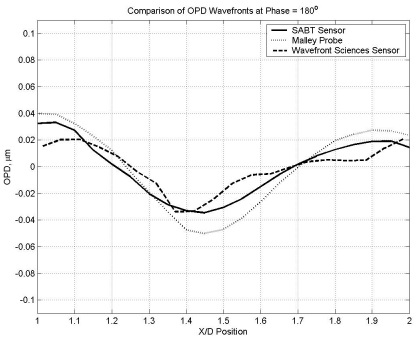

e) Phase = 180°

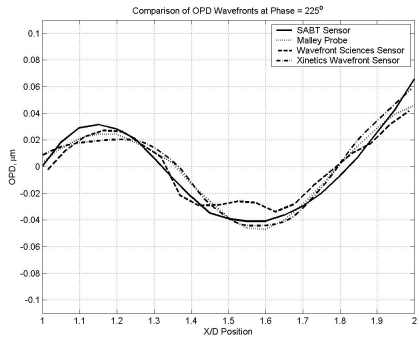

f) Phase = 225°

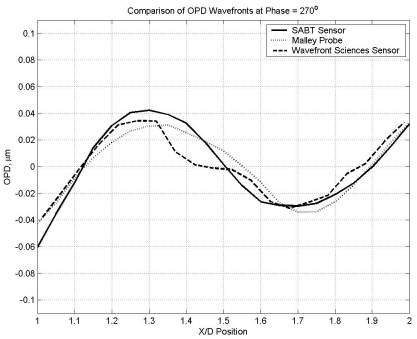

g) Phase = 270°

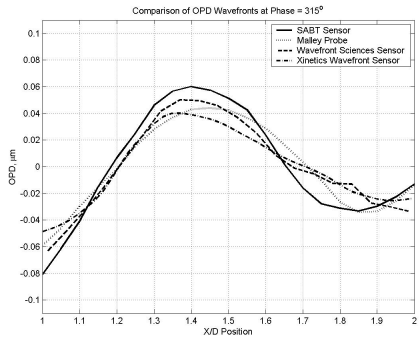

h) Phase = 315°

Figure 16. Comparison of wavefront measurement techniques: SABT sensor (solid line), Malley Probe (dotted line), Wavefront Sciences sensor (dashed line), Xinetics sensor (dash-dot line); (1.0 < X/D <2.0; OPD scale in mm).

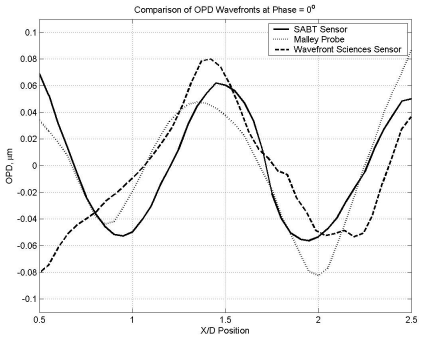

a) Phase = 0°

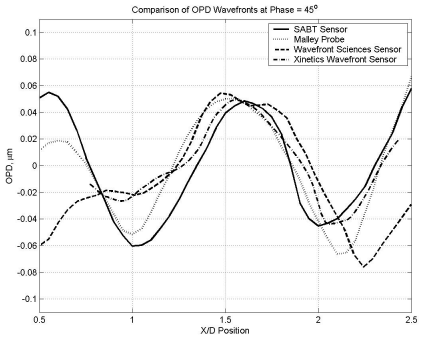

b) Phase = 45°

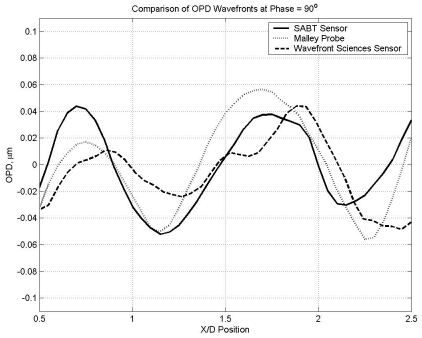

c) Phase = 90°

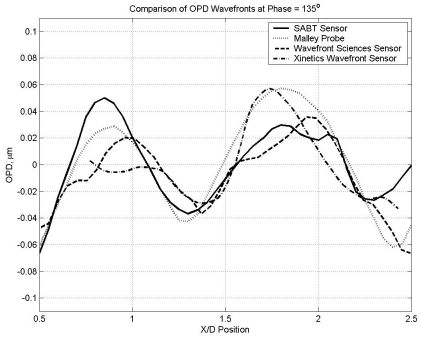

d) Phase = 135°

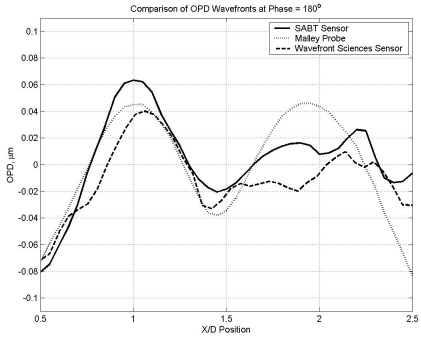

e) Phase = 180°

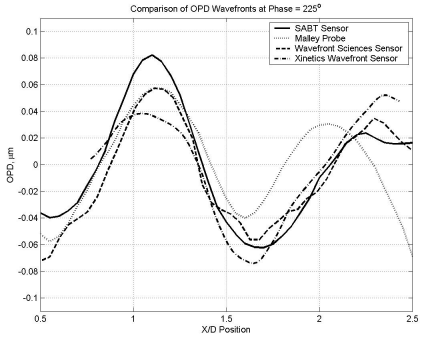

f) Phase = 225°

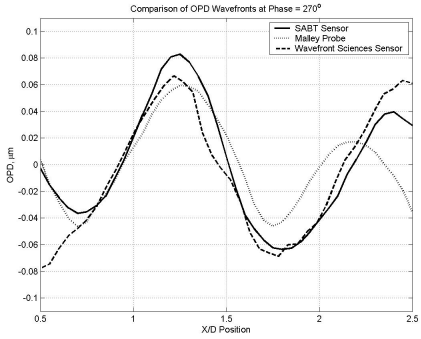

g) Phase = 270°

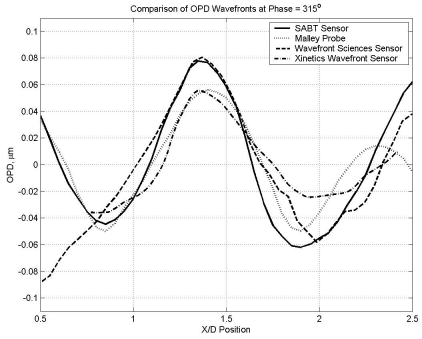

h) Phase = 315°

Figure 17. Comparison of wavefront measurement techniques (extended aperture): SABT sensor (solid line), Malley Probe (dotted line), Wavefront Sciences sensor (dashed line), Xinetics sensor (dash-dot line); (0.5 < X/D <2.5; OPD scale in mm).

V. Conclusions

As much as anything, this inter-calibration of the four wavefront sensors has demonstrated that all the methods do a good job of characterizing the aero-optic aberrating flow. In fact, the study provides a basis for confidence in the simplest technique, the Malley Probe. Differences between techniques in the actual wavefront measurements were clear consequences of the limitations of the devices; frozen-flow hypothesis breakdown, sub-aperture resolution, averaging, etc. We are left then with the inherent characteristics of the various techniques as to their choice for a particular measurement assignment. If time resolution is needed only the Malley Probe and the SABT sensors can provide these. For this flow, the Xinetics sensor has sufficient bandwidth to resolve the disturbance; however, for more-relevant, higher-speed flows the Xinetics bandwidth adds no more information than that of the Wavefront Sciences sensor. What is clearly present in the two-dimensional sensors that is not available in the SABT or Malley Probe sensors is spanwise information. Here the complementary nature of the sensors becomes important. This leads to a concept routinely practiced by the Notre Dame Aero-Optics Group and that is to approach every aero-optic problem with a complimentary suite of instruments. As our confidence in the Malley Probe has increased since our recent improvements in its software development, our suite of choice is a Malley Probe complimented by the Wavefront Sciences sensor.

Acknowledgments

These efforts were sponsored by the Air Force Office of Scientific Research, Air Force Material Command, USAF, under Grant Number F49620-03-1-0019. The U.S. Government is authorized to reproduce and distribute reprints for governmental purposes notwithstanding any copyright notation thereon. D. A. Duffin thanks the American Society of Engineering Education for their financial support with the National Defense Science and Engineering Graduate Fellowship.

References

[1]Jumper, E. J., and Fitzgerald, E. J., "Recent Advances in Aero-Optics," *Progress in Aerospace Sciences*, Vol. 37, 2001, pp. 299-339.

[2]Fitzgerald, E. J., and Jumper, E. J., "Aperture Effects on the Aero-Optical Distortions Produced by a Compressible Shear Layer," *AIAA Journal*, Vol. 40, No. 2, Feb. 2002, pp. 267-275.

[3]Fitzgerald, E. J., and Jumper, E. J., "The Optical Distortion Mechanism in a Nearly Incompressible Free Shear Layer," *Journal of Fluid Mechanics*, Vol. 512, 2004, pp. 153–189.

[4]Hugo, R. J., and Jumper, E. J., "Implications of the Homogeneous Turbulence Assumption on the Aero-Optic Linking Equation," *Optical Techniques in Fluid, Thermal, and Combustion Flow*, Vol. 2546, edited by S.S. Cha and J.D Trollinger, SPIE—International Society of Optical Engineering, Bellingham, Washington, USA, 1995, pp. 189-200.

[5]Hugo, R. J., and Jumper, E. J., "Applicability of the Aero-Optic Linking Equation to a Highly Coherent, Transitional Shear Layer," *Applied Optics*, Vol. 39, No. 24, Aug. 2000, pp. 4392-4401.

[6]Malley, M., Sutton, G. W., and Kincheloe, N., "Beam-Jitter Measurements of Turbulent Aero-Optical Path Differences," *Applied Optics*, Vol. 31, 1992, pp. 4440-4443.

[7]Hugo, R. J., and Jumper, E. J., "Quantification of Aero-Optical Phase Distortion Using the Small-Aperture Beam Technique," *AIAA Journal*, Vol. 33, No. 11, 1995, pp. 2151-2157.

[8]Hugo, R. J., and Jumper, E. J., "Experimental Measurement of a Time-Varying Optical Path Difference by the Small-Aperture Beam Technique," *Applied Optics*, Vol. 35, No. 22, Aug. 1996, pp. 4436.

[9]Hugo, R. J., Jumper, E. J., Havener, G., and Stepanek, C., "Time Resolved Aero-Optical Measurements of a Wavefront Aberrated by a Compressible Free Shear Layer," *AIAA Paper 95-1980*, Jun. 1995.

[10]Gordeyev, S., Jumper, E. J., Ng, T., and Cain, A., "Aero-Optical Characteristics of Compressible, Sub-sonic Turbulent Boundary Layers," *AIAA Paper 2003-3606*, June 2003.

[11]Hugo, R. J., "Quantifying the Spatio-Temporal Effects of Optically-Active Turbulent Flowfields on a Coherent Optical Wave," Ph.D. Dissertation, Department of Aerospace and Mechanical Engineering, University of Notre Dame, Notre Dame, IN, 1995.

[12]Duffin, D. A., Gordeyev, S., and Jumper, E. J., "Visualizing Index-of-Refraction Variations in Optically Active Flow Fields," *11th International Symposium of Flow Visualization Conference*, Paper# 075, Notre Dame, IN, 2004.

[13]Hugo, R. J., and Jumper, E. J., "Constant Current Anemometry and its impact on Aero-Optical Measurements," *AIAA Paper 95-1986*, Jun. 1995.

[14]Contact ITAC through Cain A. P.O. Box 6971, Chesterfield, MO 63006, USA.

[15]Fitzgerald, E. J., and Jumper, E. J., "Two-Dimensional Optical Wavefront Measurements Using a Small-Aperture Beam Technique Derivative Instrument," *Optical Engineering*, Vol. 39, No. 12, Dec. 2000, pp. 3285-3293.

[16]Fitzgerald, E. J., Cicchiello, J. M., Siegenthaler, J. P., and Jumper, E. J., "Optical Characterization of the Notre Dame Compressible Shear-Layer Facility," *AIAA Paper 2002-2274*, May 2002.

[17]Geary, J. M., "Introduction to Wavefront Sensors," *Tutorial texts in Optical Engineering*, Vol. TT18, Bellingham, WA, SPIE Optical Engineering Press, 1995.